A Theoretical Analysis of the Reaction between Vinyl and Acetylene: Quantum Chemistry and Solution of the Master Equation

James A. Miller*

Combustion Research Facility, Sandia National Laboratories, Livermore, California 94551-0969

Stephen J. Klippenstein

Department of Chemistry, Case Western Reserve University, Cleveland, Ohio 44106-7078

Struan H. Robertson

Molecular Simulations Inc., 240/250, The Quorum, Barnwell Road, Cambridge CB5 8RE, U.K.

Received: February 21, 2000; In Final Form: June 1, 2000

We have studied the reaction between vinyl and acetylene theoretically using electronic structure theory (DFT-B3LYP and a G2-like method) to calculate properties of stationary points on the potential, RRKM theory to compute microcanonical rate coefficients, and solutions to the *time-dependent, multiple-well* master equation to extract information about the thermal rate coefficient and product distribution as a function of temperature and pressure. For the temperature range, 300 K ≤ T ≤ 700 K, both the total rate coefficient $k_1(T,p)$ and the products are functions of pressure. For 700 K ≤ T ≤ 900 K, $k_1(T,p)$ is not always well defined in that the reactants can exhibit nonexponential decays in time. At sufficiently high pressure, the dominant product of the reaction changes from *n*-C_4H_5 to c-C_4H_5 (a four-numbered ring) to C_4H_4 + H, where C_4H_4 is vinyl acetylene, as the temperature is increased from 600 K to 900 K. For T > 900 K, the reaction can be written as an elementary step, $C_2H_3 + C_2H_2 \rightarrow C_4H_4 + H$ (R1), with a rate coefficient, $k_1 = 2.19 \times 10^{-12}T^{0.163} \exp(-8312/RT)$ cm^3/(molecule·s), *independent of pressure*, even though the intermediate collision complex may suffer numerous collisions. We interpret our results in terms of the eigenvalues and eigenvectors of the G matrix, i.e., the relaxation/reaction matrix of the master equation. For T > 900 K, $k_1(T,p)$ always corresponds to the largest eigenvalue of G, which in turn corresponds to the zero-pressure-limit rate coefficient $k_0(T)$. The situation is more complicated at lower temperatures. Our predictions are in good agreement with the limited amount of experimental information available on the reaction. The quantum chemistry calculations indicate that both c-C_4H_5 and *i*-C_4H_5 are more stable than *n*-C_4H_5. The G2-like method gives results for the $\Delta H_f^{(0)}$(0 K) of c-C_4H_5 and *i*-C_4H_5 that are lower that that of *n*-C_4H_5 by 9.5 and 11.2 kcal/mol, respectively. The DFT-B3LYP results show similar differences of 6.0 and 13.7 kcal/mol, respectively.

Introduction

Understanding the chemical mechanism governing the formation of polycyclic aromatic hydrocarbons (PAH) and soot in flames is an important practical goal in combustion chemistry. The reaction between vinyl and acetylene is potentially an important reaction in this process. One possible product, *n*-C_4H_5, can itself react with acetylene,

$$n\text{-}C_4H_5 + C_2H_2 \rightarrow C_6H_6 + H \qquad \text{(R2)}$$

to produce benzene, which may go on to form larger PAH and ultimately soot in flames. Another possible product, vinyl acetylene (C_4H_4), can also lead to cyclization through the sequence

$$C_2H_3 + C_2H_2 \rightarrow C_4H_4 + H \qquad \text{(R1d)}$$

$$C_4H_4 + H \rightarrow n\text{-}C_4H_3 + H_2 \qquad \text{(R3)}$$

$$n\text{-}C_4H_3 + C_2H_2 \rightarrow C_6H_5 \qquad \text{(R4)}$$

where C_6H_5 is phenyl. Consequently, the title reaction may be of significance in the mechanism by which PAH, some of which may be mutagenic or carcinogenic, and soot are formed during hydrocarbon combustion.

The $C_2H_3 + C_2H_2$ reaction is also a good example of a reaction where stabilization may occur over any one of 2 or 3 potential wells. Such processes are extremely important in understanding the growth of higher hydrocarbons in flames.[1] In the present investigation we consider four product channels:

$$C_2H_3 + C_2H_2 \rightarrow n\text{-}C_4H_5 \qquad \text{(R1a)}$$

$$\rightarrow i\text{-}C_4H_5 \qquad \text{(R1b)}$$

$$\rightarrow \text{c-}C_4H_5 \qquad \text{(R1c)}$$

$$\rightarrow C_4H_4 + H \qquad \text{(R1d)}$$

The c-C_4H_5 isomer above is the cyclic structure discussed by Parker and Cooksy.[2] Using density functional theory (DFT, B3LYP) and a G2-like method, we have calculated important features of the potential energy surface (PES) for the reaction, including the properties of the transition state connecting *n*-C_4H_5 to c-C_4H_5. An important byproduct of our analysis is improved

10.1021/jp000687+ CCC: $19.00
Published on Web 07/20/2000

TABLE 1: Energetics in kcal/mol Relative to Reactants for the Primary Stationary Points in the $C_2H_3 + C_2H_2$ System

species	B3LYP[a]	G2-like[b]	$\langle S^2\rangle$[c]	BAC-MP4[d]	MCSCF[e]	MRCI[f]
n-C_4H_5	−37.08	−36.31	1.272, 0.768	−37.6	−36.3	−36.3
c-C_4H_5	−43.04	−45.78	0.966, 0.782		−34.1	−40.4
i-C_4H_5	−50.81	−47.56	1.074, 0.779	−49.9	−44.4	−45.4
$C_4H_4 + H$	−1.43	−4.44		−3.8		
TS-1	5.78	5.92	1.161, 0.773	2.0		
TS-2	−6.14	−5.71	1.458, 0.801			
TS-3	2.48	2.44	0.984, 0.753	∼0.9		
TS-4a[g]	7.01	7.60	0.798, 0.759			
TS-4b[h]	7.42	9.41	1.375, 0.778			
TS-5	−0.85	−2.50	0.794, 0.755			

[a] Present B3LYP/aug-cc-pvtz calculations. [b] Present G2-like estimates to the QCISD(T)/6-311++G(3df,2pd) energies. [c] Average spin-squared for MP2/6-311++G(d,p) and B3LYP/6-31G* calculations. [d] BAC-MP4 values from ref 9. [e] MCSCF(11,11)/6-311G(d,p) values from ref 8; setting *n*-C_4H_5 values to be equivalent to G2-like energy since reference $C_2H_3 + C_2H_2$ energies are not available. [f] MRCI(7,7,43)/6-311G(d,p) values from ref 8; setting *n*-C_4H_5 values to be equivalent to G2-like energy. [g] TS-4a is the saddlepoint for the 3-centered transition state corresponding to a 1,2 H transfer connecting the *n*-C_4H_5 and *i*-C_4H_5 isomers. This is the saddlepoint used in the master equation calculations. [h] TS-4b is the saddlepoint for the 4-centered transition state corresponding to a 1,3 H transfer connecting the *n*-C_4H_5 and *i*-C_4H_5 isomers.

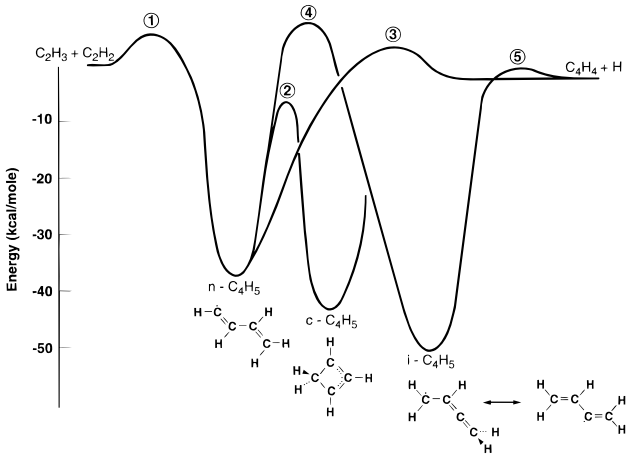

Figure 1. Reaction coordinate diagram for the $C_2H_3 + C_2H_2 \rightarrow$ products reaction.

thermochemistry for the three C_4H_5 isomers (*n*-C_4H_5, *i*-C_4H_5, and c-C_4H_5). However, using this information we have gone on to predict the total rate coefficient $k_1(T,p)$ and the product distribution as a function of temperature, T, and pressure, p, by solving the one-dimensional, time-dependent, multiple-well master equation.

To date there are relatively few experimental investigations[3−6] of the $C_2H_3 + C_2H_2$ reaction and only one theoretical one, that due to Wang and Frenklach.[7] The latter authors used an RRKM analysis, with a pseudo strong-collider assumption, to predict rate coefficients k_{1a}, k_{1b}, and k_{1d} for reactions R1a, R1b, and R1d, respectively. Our analysis is a rather substantial extension of this work.

Theory

Figure 1 is a reaction coordinate diagram for the PES on which our analysis is based, drawn from the electronic-structure calculations described below. Our objective is to predict as a function of temperature and pressure the total rate coefficient and the product distribution.

Quantum Chemistry. The relative energies of the various C_4H_5 isomers have recently been examined with a wide variety of quantum chemical methods, including B3LYP density functional theory, multiconfiguration self-consistent field (MCSCF) theory, coupled cluster theory, and multireference configuration interaction (MRCI).[8] Somewhat earlier Melius provided a BAC-MP4 analysis of many of these isomers as well as the saddlepoints connecting *n*-C_4H_5 with reactants and products.[9] The present quantum chemical calculations build on these two works with a G2-like analysis[10−12] of the energetics and a B3LYP density functional theory[13] analysis of the vibrational frequencies for the equilibrium and saddlepoint structures of importance in the $C_2H_3 + C_2H_2$ kinetics.

To start, the stationary point geometries and vibrational frequencies were obtained with B3LYP/6-31G* calculations. Subsequent energetic evaluations were performed at these B3LYP/6-31G* geometries, with both the B3LYP density functional employing the augmented correlation consistent polarized valence triple-ζ basis of Dunning and co-workers[14] and with a G2-like theory. The present G2-like theory couples QCISD(T)/6-311++G(p,d) evaluations with MP2/6-311++-(3df,2pd) and MP2/6-311++G(d,p) evaluations to obtain approximate QCISD(T)/6-311++G(3df,2pd) estimates:

$$E[\text{QCISD(T)/6-311++G(3df,2pd)}] \cong E[\text{QCISD(T)/6-311++G(d,p)}] + E[\text{MP2/6-311++G(3df,2pd)}] - E[\text{MP2/6-311++G(d,p)}] + E^{(0)} \quad (1)$$

where $E^{(0)}$ is the zero-point vibrational energy. The GAUSSIAN98 software package[15] was employed in these evaluations.

The present quantum chemical estimates for the energies of the stationary points depicted in Figure 1 are reported in Table 1, together with related values from refs 8 and 9. The results for a few additional stationary points are provided in Table 2. The B3LYP, BAC-MP4, and G2-like results are in close correspondence, differing by 5 kcal/mol or less. In contrast, the MRCI and MCSCF results deviate from the G2-like energies by as much 10 kcal/mol. Such deviations are not surprising for the MCSCF results, given that there is no treatment of dynamical correlation in this method. Furthermore, the deviations from the MRCI results may simply be an indication of the limitations in the restricted set of excitations considered in the CI part of the calculation. In particular, the MRCI calculation of ref 8 does not even include all single and double excitations from the valence orbitals as in a standard CI singles and doubles calculation.

B3LYP/6-31G* estimates have also been obtained for a number of structures differing essentially by only their torsional degrees of freedom. Such estimates are employed in obtaining the parameters for the hindered rotor treatments of these torsional modes.

Of course, there are expected to be a number of other saddlepoints connecting various local minimum structures. For

TABLE 2: Energetics in kcal/mol Relative to Reactants for Additional Stationary Points in the $C_2H_3 + C_2H_2$ System

species	B3LYP[a]	G2-like[b]	$\langle S^2\rangle$[c]	BAC-MP4[d]	MCSCF[e]	MRCI[f]
CH_3CHCCH	−48.41	−47.40	0.971, 0.771	−48.2	−51.6	−56.77
CH_3CCCH_2	−52.12	−49.85	0.953, 0.771	−49.9	−53.9	−59.33
CH_2CH_2CCH		−33.94	0.763, 0.754		−39.5	−42.40
TS-6[g]	−1.20	−4.37	0.750, 0.750			
TS-7[h]	−0.38	5.12	1.052, 0.774			

[a] Present B3LYP/aug-cc-pvtz calculations. [b] Present G2-like estimates to the QCISD(T)/6-311++G(3df,2pd) energies. [c] Expectation value of the electron spin squared for MP2/6-311++G(d,p) and B3LYP/6-31G* calculations. [d] BAC-MP4 values from ref 9. [e] MCSCF(11,11)/6-311G(d,p) values from ref 8. [f] MRCI(7,7,43)/6-311G(d,p) values from ref 8. [g] TS-6 corresponds to the saddlepoint for loss of an H from CH_3CHCCH. [h] TS-7 corresponds to the saddlepoint for a 1,2 H transfer connecting *i*-C_4H_5 with CH_3CCCH_2.

example, a 3,1 H transfer should connect *n*-C_4H_5 with CH_3-$CHCCH$. However, our attempts to locate this saddlepoint led to a structure in which the H atom was at such large separations (i.e., $r_{CH} > 3.5$ Å) that it had in essence already dissociated. It is not clear that such a long-range saddlepoint would be of any dynamical significance for the vinyl + acetylene reaction. Other difficulties were encountered in locating a number of the other expected saddlepoints. However, such saddlepoints should be irrelevant for the present two- and three-well calculations. Furthermore, of the additional wells, only the CH_3CCCH_2 well is expected to be of any kinetic significance. Some discussion of the possible contribution of that well is provided below.

Formulation and Solution of the Master Equation. To analyze the kinetics of the $C_2H_3 + C_2H_2$ reactions in detail, we must consider the time-dependent, multiple-well master equation,[16−22] which for our purposes takes the form of 3 coupled integro-differential equations:

$$\frac{dn_i(E)}{dt} = Z\int_{E_{0i}}^{\infty} P_i(E,E')n_i(E')\,dE' - Zn_i(E) - \sum_{j\neq i}^{M} k_{ji}(E)n_i(E) + \sum_{j\neq i}^{M} k_{ij}(E)n_j(E) - k_{di}(E)n_i(E)\delta_{i1} + K_{eqi}k_{di}(E)F_i(E)n_R n_m \delta_{i1} - k_{pi}(E)n_i(E) \quad i = 1, ..., M \quad (2)$$

In these equations, t is the time, E is the total internal energy, Z is the collision number per unit time, $n_i(E)\,dE$ is the number density of molecules (or complexes) in well i with energy between E and $E + dE$, E_{0i} is the ground-state energy for well i, M is the number of wells (3 in the present case), $P_i(E,E')$ is the probability that a molecule in well i with energy between E' and $E' + dE'$ will be transferred by collision to a state with energy between E and $E + dE$, $k_{ij}(E)$ is the unimolecular (RRKM) rate coefficient for isomerization from well j to well i, $k_{di}(E)$ and $k_{pi}(E)$ are the unimolecular (RRKM) rate coefficients for dissociation from well i to reactants and products respectively, n_R and n_m are the number densities of the two reactants (C_2H_3 and C_2H_2 in the present case), and K_{eqi} is the equilibrium constant for the addition reaction between the reactants and the molecule designated as well i. We have included the Kronecker delta δ_{i1} to emphasize that only well 1 (*n*-C_4H_5) can be formed directly from reactants in the present case. The function $F_i(E)$ is the equilibrium energy distribution in well i at temperature T,

$$F_i(E) = \rho_i(E)e^{-\beta E}/Q_i(T) \quad (3)$$

where $\rho_i(E)$ is the density of states of the ith well, $Q_i(T)$ is its partition function, $\beta = 1/(k_B T)$, and k_B is Boltzmann's constant.

For the present investigation we have restricted our attention to cases where helium is the bath gas. Moreover, we consider only conditions typical of experiments that seek to study radical−molecule reactions, i.e.

$$n_{He} \gg n_m \gg n_R \quad (4)$$

where m denotes molecule and R denotes radical. For such a situation $n_m \approx$ constant, and we need only append to the master equation an equation for n_R,

$$\frac{dn_R}{dt} = \int_{E_{01}}^{\infty} k_{d1}(E)n_1(E)\,dE - K_{eq1}\int_{E_{01}}^{\infty} k_{d1}(E)F_1(E)n_R n_m\,dE \quad (5)$$

The form of eqs 2 and 5 assumes that the reactants are maintained in a thermal distribution throughout the course of the reaction. Such a situation is also strongly implied by the inequalities 4.

The function $P(E,E')$ is related to $P(E',E)$ by the detailed balance condition,

$$P_i(E',E)F_i(E) = P_i(E,E')F_i(E') \quad (6)$$

Similarly, $k_{ij}(E)$ is related to $k_{ji}(E)$ by the relation

$$k_{ij}(E)\rho_j(E) = k_{ji}(E)\rho_i(E) \quad (7)$$

Letting $F_i(E)Q_i(T) = f_i^2(E)$, we can express eqs 6 and 7 as

$$\frac{f_i(E)}{f_i(E')}P_i(E',E) = \frac{f_i(E')}{f_i(E)}P_i(E,E') \quad (8)$$

and

$$k_{ij}(E)\frac{f_j(E)}{f_i(E)} = k_{ji}(E)\frac{f_i(E)}{f_j(E)} \quad (9)$$

respectively.

Let $x_R(t) = n_R(t)/n_R(0)$, $x_i(E,t) = n_i(E,t)/n_R(0)$, and $y_i(E,t) = x_i(E,t)/f_i(E)$. Then, if one divides by $n_R(0)f_i(E)$, eq 2 becomes

$$\frac{dy_i(E)}{dt} = Z\int_{E_{0i}}^{\infty}\left\{P_i(E,E')\frac{f_i(E')}{f_i(E)} - \left[1 + \frac{\sum_{j\neq i}^{M} k_{ji}(E) + k_{di}(E)\delta_{i1}}{Z}\right]\delta(E-E')\right\}y_i(E')\,dE' + \sum_{j\neq i}^{M} k_{ij}(E)\frac{f_j(E)}{f_i(E)}y_j(E) + K_{eqi}k_{di}(E)f_i(E)x_R n_m \delta_{i1} - k_{pi}(E)y_i(E) \quad i = 1, ..., M \quad (10)$$

From the detailed balance conditions (8) and (9), one can see that eq 10 is symmetric in E and E' and in i and j. By this we mean that the coefficient of $y_i(E')$ in eq 10 is identical to the coefficient of $y_i(E)$ in an analogous equation for $dy_i(E')/dt$, i.e., for any specific values of E and E'. Likewise, the coefficient of $y_j(E)$ in (10) is the same as the coefficient of $y_i(E)$ in an analogous equation for $dy_j(E)/dt$ for any values of i and j.

Multiplying eq 5 by $(K_{eq1}n_m)^{1/2}/n_R(0)$, we obtain

$$\frac{d}{dt}[(K_{eq1}n_m)^{1/2}x_R] = (K_{eq1}n_m)^{1/2}\int_0^\infty k_{d1}(E)f_1(E)dE - x_R(K_{eq1}n_m)^{3/2}\int_0^\infty k_{dl}(E)F_1(E)dE \quad (11)$$

Approximating the integrals in eq 11 as sums and rearranging,

$$\frac{d}{dt}\left[\left(\frac{K_{eq1}n_m}{\delta E}\right)^{1/2}x_R\right] = \sum_{l=1}^{N_1} y_1(E_l)(K_{eq1}n_m\delta E)^{1/2}f_1(E_l)k_{dl}(E_l) - x_R(K_{eq1}n_m)^{3/2}(\delta E)^{1/2}\sum_{l=1}^{N_1}k_{d1}(E_l)F_1(E_l) \quad (12)$$

where N_1 is the number of grid points in the energy space of well l, and δE is the spacing between grid points. Similarly, if we write eq 10 as a sum, the next-to-last term in the component equation for $dy_1(E_l)/dt$ can be written as

$$\left(\frac{K_{eq1}n_m}{\delta E}\right)^{1/2}x_R[(K_{eq1}n_m\delta E)^{1/2}f_1(E_l)k_{dl}(E_l)] \quad (13)$$

Now the coefficient of $y_1(E_l)$ in eq 12 is the same as that of

$$\left(\frac{K_{eq1}n_m}{\delta E}\right)^{1/2}x_R$$

in (13).

With the symmetrization introduced above the problem can be posed (in Dirac notation) simply as

$$\frac{d}{dt}|w(t)\rangle = G|w(t)\rangle \quad (14)$$

where $|w(t)\rangle$ is the vector of unknowns,

$$|w(t)\rangle \rightarrow \left[y_1(E_{01}), \ldots y_1(E_l), \ldots y_i(E_{0i}), \ldots y_i(E_l), \ldots \left(\frac{K_{eq1}n_m}{\delta E}\right)^{1/2}x_R\right]^T$$

and the operator G in our discrete energy basis is a real, symmetric (Hermitian) matrix. Equation 14 has the solution

$$|w(t)\rangle = \sum_{j=1}^{N_1 + \ldots N_M + 1} e^{\lambda_j t}|g_j\rangle\langle g_j|w(0)\rangle \quad (15)$$

where λ_j and $|g_j\rangle$ are the $1 + \sum_{i=1}^{M}N_i$ (negative) eigenvalues and eigenvectors of G, $|w(0)\rangle$ in the present case corresponds to $x_R(0) = 1$, and N_i is the number of grid points in the energy space of well i. We use the DSYEV routine from LAPACK[16] to diagonalize G.

From the solution vector $|w(t)\rangle$ we can extract information about the relative populations $x_R(t)$, $X_i(t)$, and $x_p(t)$, where

$$X_i(t) = \int_{E_{0i}}^\infty x_i(E,t)\,dE \quad (16)$$

$$x_p(t) = 1 - x_R(t) - \sum_{i=1}^{M}X_i(t) \quad (17)$$

In the present case $x_p(t)$ is

$$x_p(t) = \frac{n_{C_4H_4}(t)}{n_{C_2H_3}(0)} = \frac{n_H(t)}{n_{C_2H_3}(0)} \quad (18)$$

i.e. the fraction of the initial reactant concentration that has formed bimolecular products at time t.

In interpreting our results, we calculate a time-dependent rate coefficient $k_1(T,p,t)$, which we define to be

$$k_1(T,p,t) = -\frac{1}{n_{C_2H_2}x_{C_2H_3}(t)}\frac{dx_{C_2H_3}(t)}{dt} \quad (19)$$

If all the vinyl ultimately reacts (it does in all the cases considered in this investigation) and we have good exponential decays, $k_1(T,p,t) = k_1(T,p)$ (the total rate coefficient) is constant in time. Note that this will generally be the case only if one term in eq 15 (i.e. one eigenvalue/eigenvector pair) dominates the time evolution of $x_{C_2H_3}$. In cases where there are multiple-exponential decays, we characterize the rate using eq 19 at the time when $x_{C_2H_3} = 0.5$. When there is any ambiguity in the product distribution, we define

$$\alpha_n = X_1(\tau) = X_n(\tau)$$
$$\alpha_c = X_2(\tau) = X_c(\tau)$$
$$\alpha_i = X_3(\tau) = X_i(\tau)$$
$$\alpha_{bi} = x_p(\tau) \quad (20)$$

where τ is the time when $x_{C_2H_3} = 0.01$ and the α's denote the branching fractions for formation of the n, c, and i isomers and the bimolecular products. The particular times chosen to characterize the rate and products are somewhat arbitrary, but the intent simply is to define some "average" decay constant and the products formed "directly" from the reactants.

In all our master equation calculations we use a standard exponential-down model for the energy transfer function $P(E,E')$ with $\langle\Delta E_d\rangle = 200$ cm^{-1}. All the calculations were done with VARIFLEX.[24]

Microcanonical Rate Coefficients, State Counting, and Hindered Rotors. All the transition states of interest in the present investigation are tight (see Figure 1); i.e., they involve pronounced intrinsic potential energy barriers along the reaction path. Consequently, we can use conventional transition-state theory[1] to evaluate the microcanonical rate coefficients that appear in the master equation. Under the constraints of the RRKM approximation,[1] any one of the dissociation or isomerization rate coefficients appearing in eq 2 can be written as

$$k(E) = \frac{N_j^{\ddagger}(E)}{h\rho_i(E)} \quad (21)$$

where $N_j^{\ddagger}(E)$ is the sum of states for transition state j with energy less than or equal to E and h is Planck's constant. We evaluate $N_j^{\ddagger}(E)$ and $\rho_i(E)$ as $N_j^{\ddagger}(E) = \sum_J(2J+1)N_j^{\ddagger}(E,J)$ and $\rho_i(E) = \sum_J(2J+1)\rho_i(E,J)$, where $N_j^{\ddagger}(E,J)$ is the sum of states for

transition state j with energy less than or equal to E and total angular momentum quantum number equal to J (analogous definition for $\rho_i(E,J)$). The $N_j^{\ddagger}(E,J)$ and $\rho_i(E,J)$ functions are computed rigorously by methods similar to those described previously.[25−27] The present formulation does not conserve angular momentum. However, angular momentum conservation is not expected to be as important in cases such as this one, with all tight transition states, as it might be with several loose ones, i.e., transition states with no intrinsic potential energy barriers.[1,34,35] In the latter case "threshold energies" can change significantly with J; in the former case they usually do not.

There are a few vibrational degrees of freedom in the transition states and molecules (or complexes) depicted in Figure 1 that cannot be modeled accurately as harmonic oscillators. These modes mostly, but not always, are low-frequency torsional motions involving internal rotations about C−C single bonds. We model all nonharmonic vibrations as one-dimensional hindered rotors. First we calculate the classical density of states

$$\rho_{cl}(E) = \frac{\sqrt{2I_R}}{h}\int_0^{2\pi} H[E - V(\varphi)][E - V(\varphi)]^{-1/2}\,\mathrm{d}\varphi \quad (22)$$

where φ is the angle of rotation, $H(x)$ is the Heaviside step function, $V(\varphi)$ is the hindering potential, and I_R is the reduced moment of inertia. We compute I_R by the method proposed by Pitzer (eq 1 of ref 28). Then we approximate the corresponding quantum density by

$$\rho_q(E) = \rho_{cl}(E)\frac{\rho_q^{(ho)}(E)}{\rho_{cl}^{(ho)}(E)} \quad (23)$$

where ho denotes harmonic oscillator, i.e., the Pitzer−Gwinn[29] approximation. Finally, we convolve the hindered-rotor quantum densities successively with the harmonic sum or density of states to get the total vibrational sum or density of states. Partition functions are computed similarly.

To perform the integration indicated in eq 22 we must have a hindering potential. We calculate the properties of $V(\varphi)$ directly using DFT and then approximate it by a truncated Fourier cosine series, either

$$V(\varphi) = V_0 + V_1\cos(m\varphi) \quad (24)$$

or

$$V(\varphi) = V_0 + V_1\cos(m\varphi) + V_2\cos(2m\varphi) \quad (25)$$

where m is an integer. In VARIFLEX,[24] which we use for all the calculations, a rotor whose potential is given by eq 24 is termed a type 1 rotor. For this case $V(\varphi = \pi/m)$, a barrier height, must be specified along with m. $V(0)$ is always assumed to be zero, i.e., the equilibrium point. When eq 25 is used to approximate $V(\varphi)$, we distinguish two types of rotors. For a type 2 rotor, along with m we specify $V(\pi/m)$ and the force constant at $\varphi = 0$. For a type 3 rotor, we specify $V(\pi/2m)$ and $V(\pi/m)$, i.e., a barrier height and the potential at a second minimum.

Table 3 contains all the PES information used in our calculations, including the hindered rotor properties.

Results and Discussion

Our principal objective in this investigation is to inquire into how temperature and pressure affect the formation of the different products of the $C_2H_3 + C_2H_2$ reaction shown in Figure 1, i.e., the various C_4H_5 isomers and the bimolecular $C_4H_4 + H$ channel. However, we are also interested in the total rate

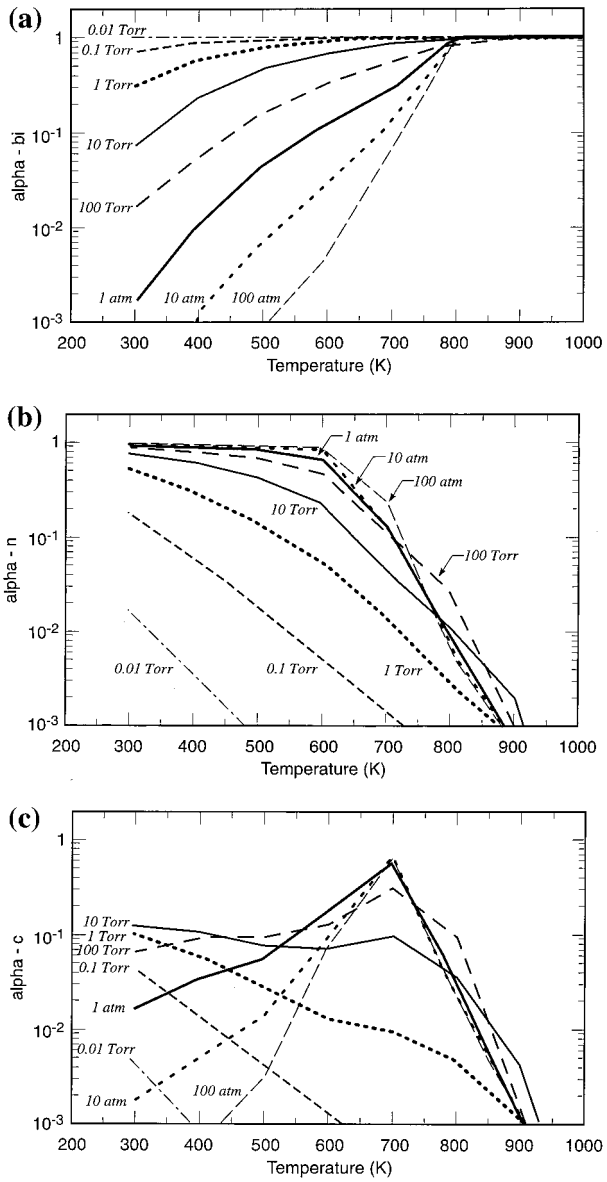

Figure 2. Product distribution as a function of temperature and pressure from the *two-well* master equation model using the DFT-B3LYP PES energies: (a) $C_4H_4 + H$; (b) *n*-C_4H_5; (c) c-C_4H_5.

coefficient $k_1(T,p)$. In most of our calculations we neglect the possibility that *n*-C_4H_5 can isomerize to *i*-C_4H_5 (TS-4 in Figure 1) and thus pose the problem as one involving only 2 potential wells. This reduces the strain on our computing resources and allows us to use a relatively small value of the bin width, $\delta E = 50$ cm^{-1}. This approximation is justified quantitatively below by solving the full three-well problem for one set of potential parameters with a $\delta E = 100$ cm^{-1}. Except for one set of calculations we have used a barrier height for TS-1, E_{b1}, of 5.72 kcal/mol (2000 cm^{-1}), which is inconsequentially different from the DFT and G2-like results shown in Table 1.

Product Distribution. Figures 2−4 show results for the various branching fractions (α_{bi}, α_n, α_c, α_i)as a function of temperature and pressure computed from the master equation with the DFT (2 wells), DFT (3 wells), and G2-like (2 wells) barrier heights and well depths, respectively. By comparing Figures 2 and 4, one can see that it makes no significant difference which set of barrier heights we use—they are practically the same anyway. Therefore, the remainder of our discussion refers to the DFT calculations as our base case. Likewise, comparing Figures 2 and 3 shows that isomerization

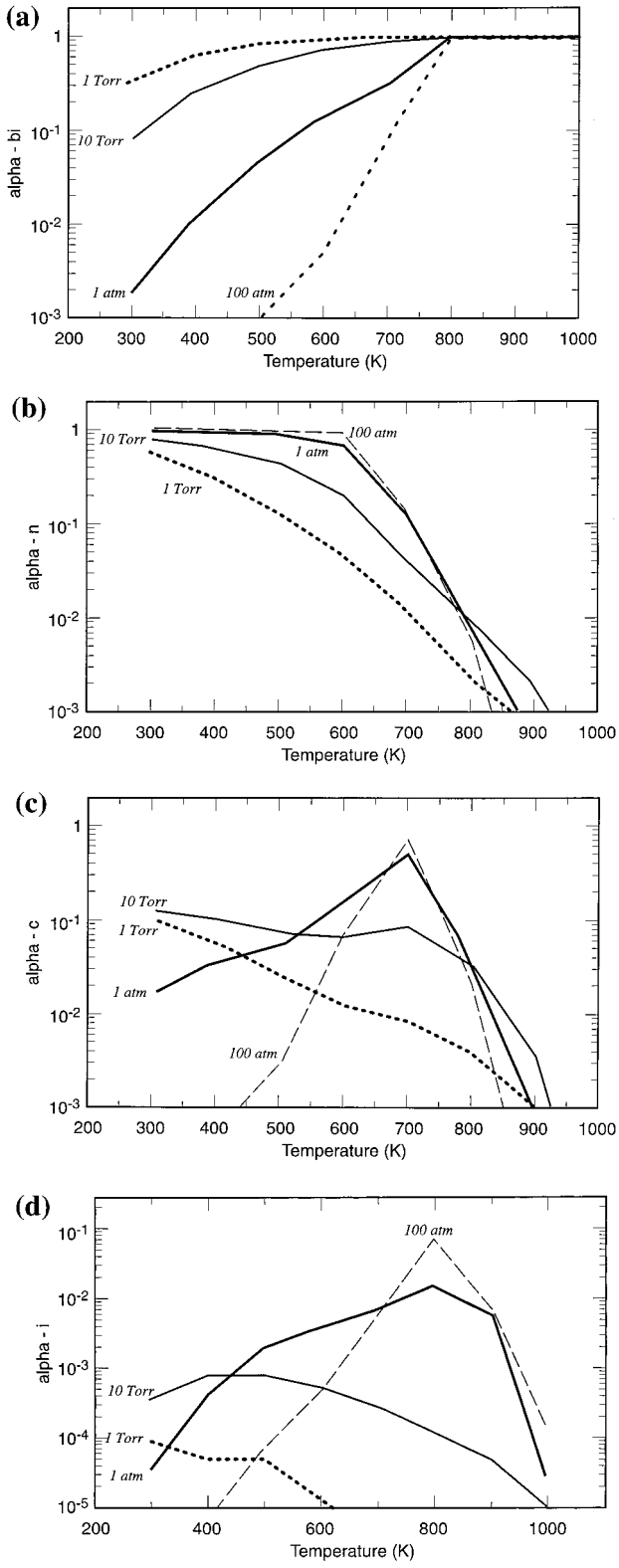

Figure 3. Product distribution as a function of temperature and pressure from the *three-well* master equation model using the DFT-B3LYP PES energies: (a) $C_4H_4 + H$; (b) *n*-C_4H_5; (c) c-C_4H_5; (d) *i*-C_4H_5.

of *n*-C_4H_5 to *i*-C_4H_5 is not a very significant process in general and treating the reaction as a two-well problem is quite satisfactory. However, it is interesting that at sufficiently high pressure it is possible to stabilize as much as 5% of the initial vinyl concentration in the *i*-C_4H_5 well at $T \approx 800$ K. At lower temperatures, the barrier for TS-4 restricts the amount of isomerization that can occur from the *n*-C_4H_5 well, and at higher

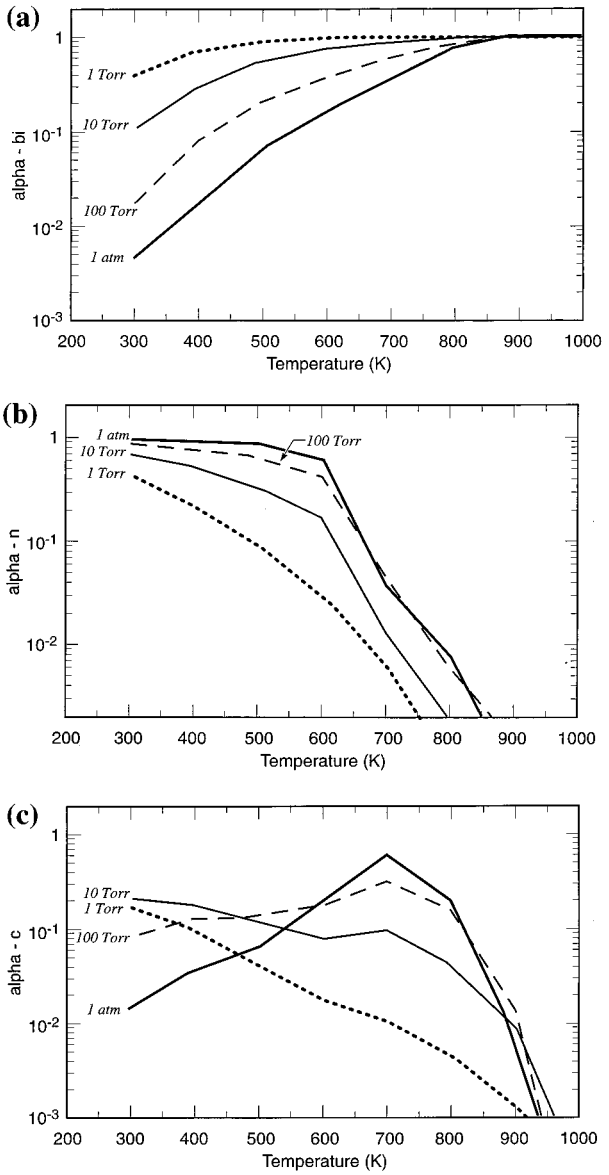

Figure 4. Product distribution as a function of temperature and pressure from the two-well master equation model using the *G2-like* PES energies: (a) $C_4H_4 + H$; (b) *n*-C_4H_5; (c) c-C_4H_5.

temperatures *i*-C_4H_5 becomes collisionally (or thermodynamically) unstable in that the net effect of collisions is to dissociate it into $C_4H_4 + H$ on a time scale smaller than that governing the time evolution of $x_R(t)$. We discuss this point more below. The inclusion of the CH_3CCCH_2 well, as a fourth well, would be expected to have a qualitatively similar effect to that observed for the inclusion of the third well. However, the net effect would likely be somewhat larger since the overall well depth is slightly greater, the barrier from the third well is somewhat lower, and the vibrational frequencies in the fourth well are somewhat lower. As a result, the dissociation from the fourth well would require a higher temperature than that from the third well. Correspondingly the range of temperature for which there is significant population in the fourth well should be greater, and the peak population in that well should also be slightly greater. However, since the increase in the well depth is only 2 kcal/mol, the increase in these quantities should be quite minor.

Figures 2−4 show the same general trends in the branching fractions. At all pressures α_{bi} increases with increasing temperature until, above $T \approx 900$ K, $\alpha_{bi} \approx 1$ *independent of pressure*. At the same time α_n decreases continuously with

increasing T, although at high pressures $\alpha_n \approx 1$ up to a temperature of about 600 K, after which it begins to drop off rapidly. The situation with α_c is more complicated. At low pressures α_c decreases continuously with *T*, whereas at sufficiently high *p* it first increases up to a temperature of $T \approx$ 700 K and then drops off as temperature increases further.

The behavior of α_c can be understood as follows. At low pressures, collisions are relatively rare events for any of the C_4H_5 complexes, and the complex resulting from any particular collision is likely to roam freely over both the *n*-C_4H_5 and c-C_4H_5 wells for a long time before it is either stabilized or dissociates to products or back into reactants. As the temperature increases the complex lifetime decreases faster than the collision rate increases, and less stabilization occurs. By contrast, at high pressure the initial *n*-C_4H_5 complex suffers numerous collisions before it can isomerize or dissociate, and at low temperature, stabilization to *n*-C_4H_5 is the dominant outcome. However, as the temperature increases to about 700 K, activating collisions begin to compete more favorably with deactivating collisions, and more and more complexes are able to overcome the isomerization barrier and become stabilized as c-C_4H_5. Above $T \approx$ 700 K dissociation of *n*-C_4H_5 into $C_4H_4 + H$ dominates. This occurs not only because the one-way flux through TS-3 increases relative to that through TS-2 but, more importantly, because it becomes increasingly common for a complex to isomerize from *n*-C_4H_5 to c-C_4H_5, suffer a number of collisions, both deactivating and activating, and then isomerize back to *n*-C_4H_5 and ultimately dissociate to products.

For $T > 900$ K (actually even for $T > 800$ K), the $C_2H_3 + C_2H_2$ reaction forms $C_4H_4 + H$ almost exclusively, even at very high pressures, e.g. $p = 100$ atm. This is a consequence of the collisional instability of all the C_4H_5 isomers (including *i*-C_4H_5) to dissociation at high temperature. If one were to prepare an ensemble of any one of the C_4H_5 radicals at low temperature and then immerse it in a bath of helium at $T = 900$ K, the radicals would essentially all dissociate to $C_4H_4 + H$ in a time that is less than that required for all the vinyl to react in our calculations. A similar condition exists for isomerization of *n*-C_4H_5 to c-C_4H_5. At $T \approx 600$ K the *n*-C_4H_5 present at lower temperatures begins to isomerize to the more stable c-isomer, which has a very sharp peak in concentration at 700 K. Collisions always drive the system toward thermal and chemical equilibrium, and if the barriers to chemical reaction are low enough, the chemical equilibration can take place very rapidly.

Callear and Smith[3,4] performed experiments in which they prepared vinyl by the reaction of H with acetylene and monitored the products of the subsequent chain reaction. One of those products was benzene. They concluded that benzene was formed by the sequence

$$\begin{aligned} H + C_2H_2 &\rightarrow C_2H_3 \\ C_2H_3 + C_2H_2 &\rightarrow n\text{-}C_4H_5 \\ n\text{-}C_4H_5 + C_2H_2 &\rightarrow C_6H_6 + H \end{aligned} \qquad \text{(R1a)}$$

Examining Figure 1 it is not obvious that *n*-C_4H_5 should be the dominant product of (R1) under the conditions of their experiments. In fact, if we have a sufficiently low temperature and start at $p = 0$, then slowly increase the pressure, the first stabilization product that we would expect to see is c-C_4H_5, simply because c-C_4H_5 is energetically accessible and has the deepest well. Callear and Smith's experiments were performed at temperatures of 300 and 400 K and in the pressure range 100 Torr $\leq p \leq$ 500 Torr. Figure 5 is a plot of our results

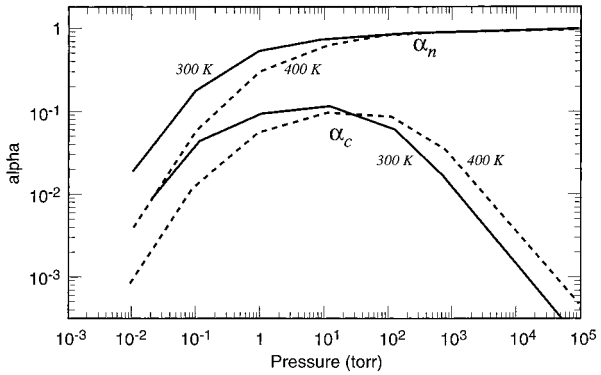

Figure 5. Pressure dependence of α_n and α_c for $T = 300$ K and T = 400 K. Two-well master equation with DFT-B3LYP PES energies.

for α_n and α_c as a function of pressure for $T = 300$ K and $T =$ 400 K. In the pressure range of interest, well over 90% of the product is *n*-C_4H_5, in agreement with the Callear and Smith interpretation. If we used H_2 as the bath gas (instead of helium) in our calculations, as was the case for the experiments, one would expect to get even more *n*-C_4H_5, because H_2 has both a higher collision rate *Z* and a larger value of $\langle \Delta E_d \rangle$ than does helium. Both of these factors should result in increased stabilization into the *n*-C_4H_5 well, more effectively robbing the c-C_4H_5 channel.

It is of interest to investigate how properties of the PES, particularly the c-C_4H_5 well depth and the TS-2 barrier height (E_{b2}), affect the branching fractions. In Figure 6 we have plotted α_{bi}, α_n, and α_c as a function of temperature, at a pressure of $p = 1$ atm, for a series of well depths: $E_{02} = -43.4$, -36.9, -31.9, and -22.9 kcal/mol. The first of these well depths is the nominal DFT value, the second corresponds to the DFT well depth for *n*-C_4H_5 (i.e. E_{01} and E_{02} are equal for this case), and the last 2 correspond to wells shallower than that for *n*-C_4H_5. Not surprisingly, shallower wells result in less c-C_4H_5 stabilization and a movement of the peak in α_c shown in Figure 6 to lower temperatures. However, the magnitude in the drop-off with decreasing well depth is somewhat suprising. The change of E_{02} from -43.4 to -36.9 kcal/mol results in a drop in the peak value of α_c from 57% to 5% and moves the peak from $T \approx 700$ K to $T \approx 600$ K. Another 5 kcal/mol reduction in well depth drops the peak to 0.5% and moves it to $T \approx 400$ K. The values of α_c for the last case are too small to be plotted in Figure 6. The "lost" c-C_4H_5 is recovered both as *n*-C_4H_5 and $C_4H_4 + H$, but predominantly the latter, particularly for $T \approx 700$ K, where c-C_4H_5 is the dominant product in the nominal case.

Figure 7 shows the effects on the product distribution of raising and lowering the isomerization barrier height, E_{b2}, by 5 kcal/mol. The most obvious and important effects are the overall increase in α_c as E_{b2} is reduced and the tendency for the peak in α_c to move to lower temperatures with smaller values of E_{b2}. The increases in c-C_4H_5 with reduced values of E_{b2} are at the expense of both *n*-C_4H_5 and $C_4H_4 + H$, but the most dramatic effect is the huge drop in α_n at $T \approx 600$ K when E_{b2} is reduced from its nominal value. The increase in α_n for the low-barrier case in going from 600 to 700 K is simply a consequence of the rate of formation of *n*-C_4H_5 from $C_2H_3 + C_2H_2$ increasing more rapidly with temperature than the rate of isomerization of *n*-C_4H_5 to c-C_4H_5.

Although small, there is another interesting effect shown in Figure 7. At $T = 300$ K, α_{bi} increases whether we raise or lower the isomerization barrier. The effect of raising the barrier is obvious: the rate of isomerization from *n*-C_4H_5 to c-C_4H_5 is reduced, thus allowing increased flux into the competing C_4H_4

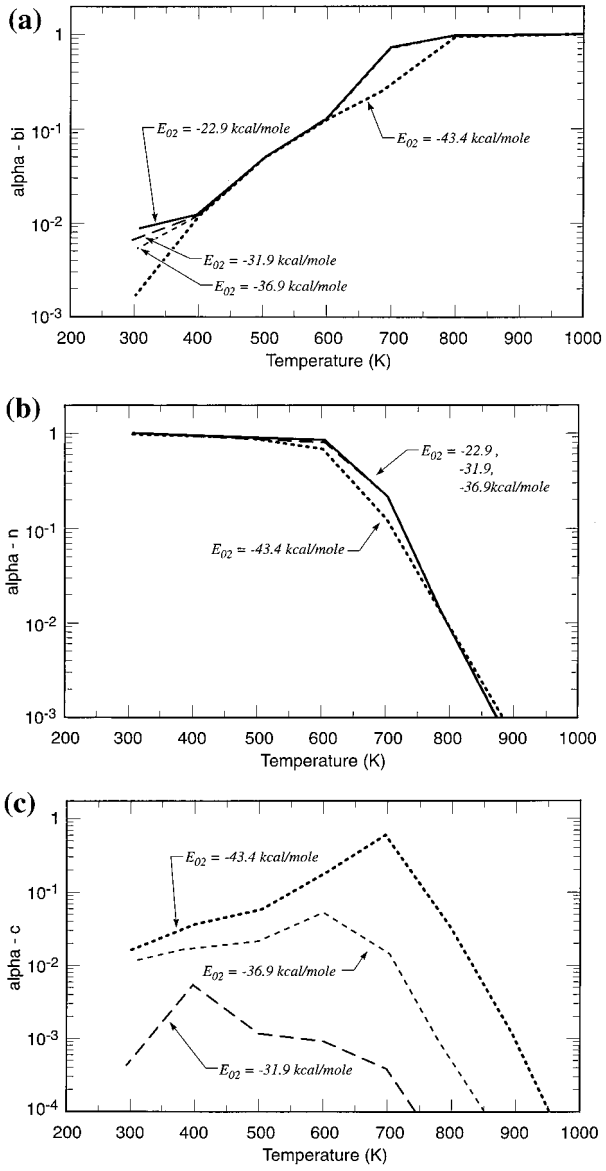

Figure 6. Effect of c-C_4H_5 well depth on product distribution at p = 1 atm. Two-well master equation with DFT-B3LYP PES energies: (a) C_4H_4 + H; (b) *n*-C_4H_5; (c) c-C_4H_5.

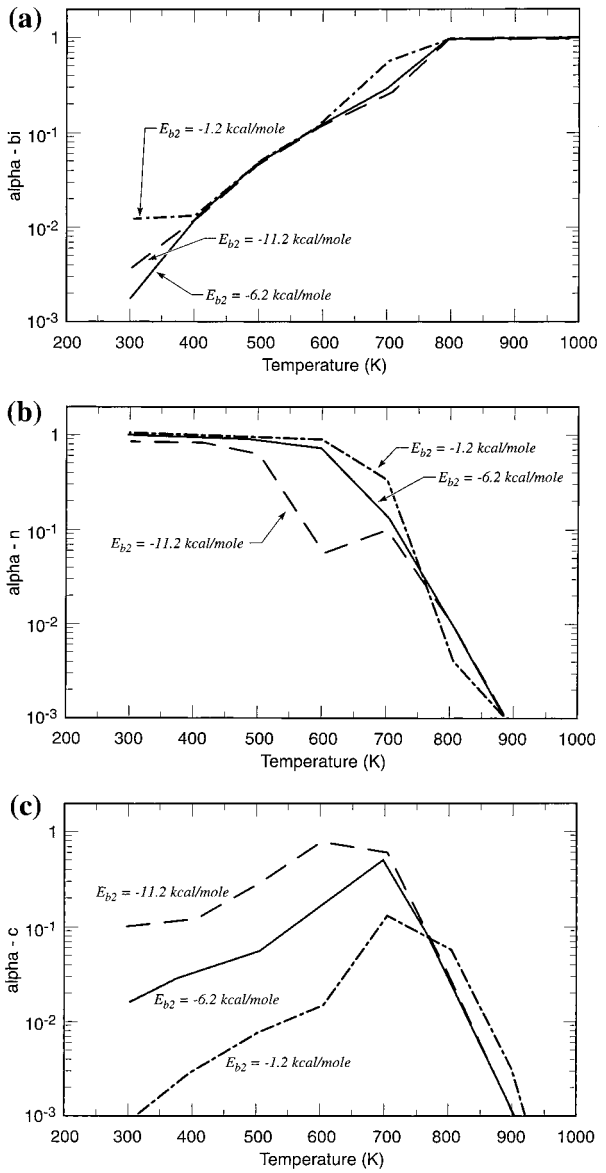

Figure 7. Effect of barrier height E_{b2} on product distribution. Two-well master equation with DFT-B3LYP PES energies: (a) C_4H_4 + H; (b) *n*-C_4H_5; (c) c-C_4H_5.

+ H channel. However, there is also another effect: reducing the barrier height allows increased "communication" between c-C_4H_5 and C_4H_4 + H. That is, reducing the barrier also results in an increased likelihood that a c-C_4H_5 complex will isomerize back to *n*-C_4H_5 and subsequently dissociate. Apparently this latter effect is the dominant one when we reduce the barrier height from its nominal value in Figure 7.

Total Rate Coefficient $k_1(T,p)$. Figure 8 consists of 2 Arrhenius plots of $k_1(T)$ for a series of pressures—the two plots are based on the same information except that Figure 8b magnifies the central part of the temperature range. Also plotted in Figure 8 are the experimental results obtained to date and the theoretical result for the high-pressure limit $k_\infty(T)$,

$$k_\infty(T) = \frac{1}{hQ_{C_2H_3}Q_{C_2H_2}}\int_0^\infty N_1^{\ddagger}(E)\,\exp(-\beta E)\,\mathrm{d}E \qquad (26)$$

All the theoretical results are based on the DFT (2-well model) potential energy surface parameters.

For any given pressure, $k_1(T)$ shows behavior that is qualitatively similar to what we observed previously in our analysis of the $C_2H_5 + O_2$ reaction.[26] At the higher pressures, $k_1(T)$ starts out near the high-pressure limit at low T. As temperature is increased, $k_1(T)$ moves farther and farther away from $k_\infty(T)$ until, for $T > 900$ K, *no matter how high the pressure*, $k_1(T)$ coalesces with $k_0(T)$, the rate coefficient at the zero-pressure limit. We have not actually plotted $k_0(T)$ in Figure 8, but the results for $p = 0.1$ Torr and $p = 0.01$ Torr are indistinguishable on the plot, indicating clearly that the zero-pressure limit has been reached at these pressures. For temperatures up to $T \approx 700$ K the rate coefficient is well defined, i.e., $k_1(T,p,t)$ defined in eq 19 is independent of time. For temperatures in the range of 700 K $\leq T \leq$ 900 K, we can have biexponential decays of $x_R(t)$, and $k_1(T,p,t)$ is not always constant in time. Above $T = 900$ K, $x_R(t)$ always decays exponentially and $k_1(T,p)$ is well defined. The time dependence of $k_1(T,p,t)$ is more pronounced the larger we make the pressure—the low-pressure cases show little or no time dependence for $k_1(T)$. Likewise, the transition of $k_1(T)$ from near $k_\infty(T)$ to $k_0(T)$ occurs more rapidly as the pressure is increased (see the $p = 100$ atm case in Figure 8). This transition in the rate coefficient occurs in the same temperature range as that where the principal

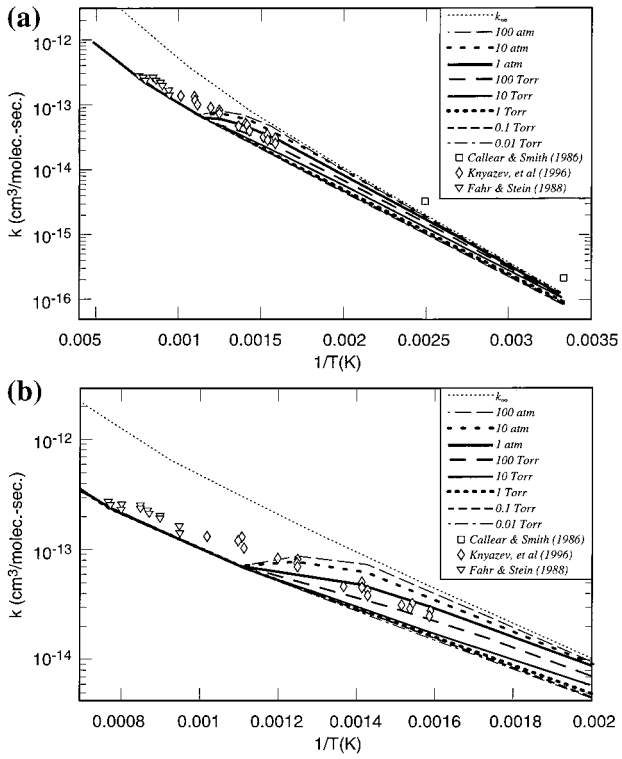

Figure 8. Arrhenius plots of $k_1(T,p)$ for the two-well master equation model using the DFT- B3LYP PES energies. Experiments are from Knyazev et al. (1996), Fahr and Stein (1988) as corrected by Knyazev et al., and Callear and Smith (1986) as corrected by Knyazev et al.

products change from *n*-C_4H_5 to c-C_4H_5 to C_4H_4 + H. Note that $k_1(T)$ is independent of pressure above 900 K *even though the intermediate complexes may suffer numerous collisions.*

At first glance, it seems quite remarkable that $k_1(T,p) \approx k_0(T)$ independent of pressure for $T > 900$ K. However, this result is a natural consequence of having a loose inlet transition state (TS-1) and a tight exit transition state (TS-3) (in this context, a "loose" transition state is characterized by lower frequencies and larger moments of inertia than a "tight" one). For temperatures greater than 900 K, the average energy transferred per collision ($\langle\Delta E\rangle$) at energies in the vicinity of TS-1 and TS-3 is quite small (indicating that activating, as well as deactivating, collisions are important), and stabilization is problematic. At the same time, reaction to C_4H_4 + H is limited by TS-3 regardless of the pressure. Under these conditions,

$$k_0(T) \propto \int_{E_{b1}}^{\infty} N_3^{\ddagger}(E) \exp(-\beta E)\, dE \qquad (27)$$

and

$$k'_\infty(T) \propto \int_{E_{b3}}^{\infty} N_3^{\ddagger}(E) \exp(-\beta E)\, dE \qquad (28)$$

where the proportionality constant in both expressions is the same as that in eq 26. Note the difference between $k_\infty(T)$ and $k'_\infty(T)$, the latter of which is the real infinite-pressure limit rate coefficient for the bimolecular channel. Thus, the difference between $k'_\infty(T)$ and $k_0(T)$ is

$$I \propto \int_{E_{b3}}^{E_{b1}} N_3^{\ddagger}(E) \exp(-\beta E)\, dE \qquad (29)$$

For the present case, at $T = 1000$ K, we get

$$I/k'_\infty(T) \approx 5 \times 10^{-4}$$

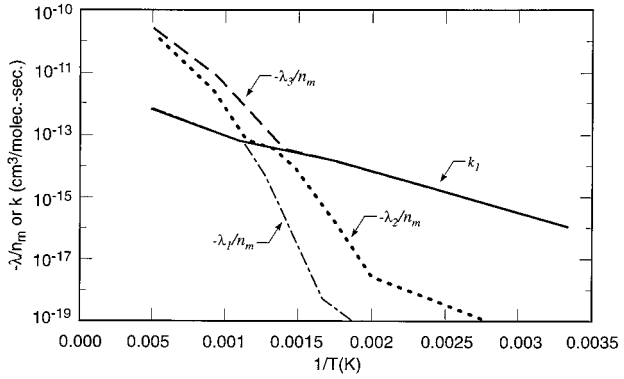

Figure 9. Arrhenius plot of "chemical" eigenvalues of G for $p = 100$ Torr.

Consequently, for practical purposes $k_0(T)$ and $k'_\infty(T)$ are the same in the high-temperature regime.

It is interesting and instructive to interpret the rate coefficient in terms of the eigenvalues and eigenvectors of G. Let λ_1 be the largest such eigenvalue (the least negative one), λ_2 the next largest, etc. At low temperatures and pressures sufficiently high that collisions play a significant role in determining the rate, three eigenvalues are much larger than the rest, and they themselves are well separated in magnitude. Under these conditions one can identify $-\lambda_3$ as the relaxation rate[30−32] for dissociation of *n*-C_4H_5 into C_2H_3 + C_2H_2, $-\lambda_2$ as that for isomerization of *n*-C_4H_5 to c-C_4H_5, and $-\lambda_1$ as that for dissociation of *n*-C_4H_5 to C_4H_4 + H. (Actually, it is probably better to think of the latter dissociation as occurring from the coupled two-well system consisting of both *n*-C_4H_5 and c-C_4H_5.) For the temperature range, 300 K < T < 700 K, the rate coefficient is determined by λ_3. As the temperature is increased from 300 to 700 K the 3 eigenvalues get closer and closer together in magnitude. For temperatures between 700 and 900 K the relationship between $k_1(T,p)$ and the three eigenvalues depends somewhat on the pressure, although the general trends are the same in all cases (except for very low pressures). We shall refer to the $p = 100$ Torr case to be specific. At 700 K, λ_2 and λ_3 become very close in magnitude, and there is a hint of biexponential decay in $x_R(t)$. At 800 K, $k_1(T,p)$ is governed predominantly by λ_2, although the decay in $x_R(t)$ is not perfectly exponential. At 900 K, λ_1 and λ_2 have similar magnitudes, and again there is biexponential decay in $x_R(t)$. By 1000 K, $x_R(t)$ has become perfectly exponential with the relaxation rate $-\lambda_1$. For $T \geq 1000$ K, $k_1(T,p)$ is always determined by λ_1, the largest eigenvalue of G. This occurs almost simultaneously with the coalescence of $k_1(T,p)$ with $k_0(T)$.

The behavior described in the previous paragraph is shown graphically in Figure 9. At low temperatures $k_1 = -\lambda_3/n_m$ and at high temperatures $k_1 = -\lambda_1/n_m$. In the temperature range 700 K < T < 900 K, the three curves lie very close together, leading to nonexponential decays in $x_R(t)$. It is interesting that $-\lambda_3/n_m$ above the k_1 curve appears to be the natural extension of $-\lambda_2/n_m$ from below the k_1 curve. Similarly, $-\lambda_2/n_m$ above the k_1 curve appears to be the natural extension of $-\lambda_1/n_m$ from below k_1. Although we have not discovered it yet, there may be a universal method of categorizing the eigenvalues and eigenvectors that allows us to make the identifications just described, i.e., analogous to quantum numbers in electronic structure theory. If such were the case, k_1 would always correspond to one particular eigenvalue/eigenvector pair. However, for the moment we can think of nonexponential decays as occurring in a region of "avoided crossings" of the eigenvalue curves.

We should elaborate a little on the eigenvalue spectrum of

TABLE 3.

molecule	electronic degeneracy	symmetry no.[a]	vibrational frequencies (cm^{-1})	rotational constants (cm^{-1})	hindered rotors[b]
C_2H_2	1	2	535, 535, 776, 776, 2088, 3441, 3541	1.18	
C_2H_3	2	1	728, 814, 923, 1072, 1417, 1673, 3070, 3167, 3257	5.82, 0.928, 0.800	
n-C_4H_5	2	1	298, 513, 565, 810, 857, 930, 960, 1036, 1192, 1269, 1330, 1464, 1649, 1707, 3040, 3162, 3176, 3248, 3266	1.65, 0.151, 0.139	3, 1, 3.09, 1110, 3202, 3, 1, 34.0, 230, 3965
c-C_4H_5	2	2	394, 512, 532, 880, 899, 910, 940, 974, 1021, 1086, 1185, 1201, 1232, 1349, 1458, 1515, 3043, 3081, 3207, 3238, 3250	0.475, 0.435, 0.237	
i-C_4H_5	2	2	228, 495, 529, 576, 727, 881, 915, 940, 1000, 1102, 1209, 1398, 1480, 1518, 1930, 3098, 3135, 3154, 3182, 3278	1.39, 0.147, 0.136	3, 1, 10.7, 0.0, 1100
TS-1	2	1	133, 196, 235, 569, 768, 774, 780, 859, 932, 1093, 1422, 1666, 1986, 3080, 3155, 3250, 3427, 3512	1.06, 0.109, 9.84×10^{-2}	2, 1, 2.58, 150, 110
TS-2	2	1	452, 602, 705, 754, 779, 905, 913, 934, 1023, 1070, 1197, 1283, 1423, 1497, 1555, 3123, 3148, 3175, 3189, 3234	0.538, 0.310, 0.208	
TS-3	2	1	321, 348, 522, 540, 608, 640, 717, 891, 955, 1009, 1112, 1334, 1454, 1696, 2126, 3158, 3178, 3265, 3485	1.41, 0.149, 0.135	2, 1, 4.35, 175, 1222
TS-4	2	1	35, 224, 247, 475, 515, 723, 844, 894, 949, 1006, 1110, 1314, 1448, 1683, 1854, 2352, 3072, 3101, 3174, 3259	1.27, 0.169, 0.149	
TS-5	2	1	178, 230, 353, 560, 625, 632, 713, 902, 946, 1011, 1123, 1335, 1462, 1684, 2199, 3161, 3180, 3266, 3496	1.12, 0.143, 0.137	3, 1, 5.01, 0.0, 151

[a] Hindered rotor formulation. [b] The first 2 entries are the rotor type and the value of m (see eqs 24 and 25). The third entry is the rotational constant in cm^{-1}. For a type 2 rotor, the fourth entry is the potential (cm^{-1}) at $\varphi = \pi/m$ and the fifth is the force constant at $\varphi \neq 0$. For type 3 rotor, the fourth entry is the potential at $\varphi = \pi/m$, and the fifth is the potential at $\varphi = \pi/2m$.

G. In general, one should expect a chemically significant eigenvalue for each transition state. We have identified the chemical processes associated with the λ's in the present case from 2 observations: (1) By following the long-time behavior of the system under the appropriate conditions (low temperature), one can see first the decay of the reactants as $X_n(t)$ rises during a period when the time evolution is controlled by λ_3, then a rise of $X_c(t)$ and fall of $X_n(t)$ when the time evolution is controlled by λ_2, and finally the rise of $x_p(t)$ and fall of both $X_c(t)$ and $X_n(t)$ while λ_1 controls the rate. (2) We have varied the barrier heights E_{b1}, E_{b2}, and E_{b3} and inquired about the effects of such changes on the eigenvalues. Varying E_{b1} changes λ_3, leaving λ_2 and λ_1 relatively unscathed. Similarly, a change in E_{b2} modifies the value of λ_2, and a change in E_{b3} changes the value of λ_1, with the values of the remaining eigenvalues staying more or less the same. These identifications were made at temperatures below the "avoided crossings" region in Figure 9. At high temperature, changing E_{b2} causes a change in λ_3, so that if one identifies an eigenvalue with a transition state, the λ_2,λ_3 avoided crossing in Figure 9 becomes a real crossing. However, the λ_1,λ_2 interaction remains an avoided crossing. In principle, using the three eigenvalues and the appropriate equilibrium constants, we should be able to compute thermal rate coefficients for the corresponding isomerization and dissociation/recombination reactions, at least under conditions where the λ's are significantly different in magnitude.[32,33] However, such an analysis is beyond the scope of the present work. We simply want to identify the λ's as characteristic time constants for the chemical processes noted.

The agreement of our predictions for $k_1(T,p)$ with experiment shown in Figure 8 is reasonably good, although it can certainly be improved. Bear in mind that the Callear and Smith experiments were conducted at pressures greater 100 Torr, whereas those of Fahr and Stein were in the 1−10 mTorr range and those of Knyazev et al. were at pressures of roughly 3−10 Torr. Unlike the predictions of Wang and Frenklach,[7] our rate coefficient is slightly pressure-dependent at room temperature and becomes increasingly so as T increases up to $T \approx 700$ K.

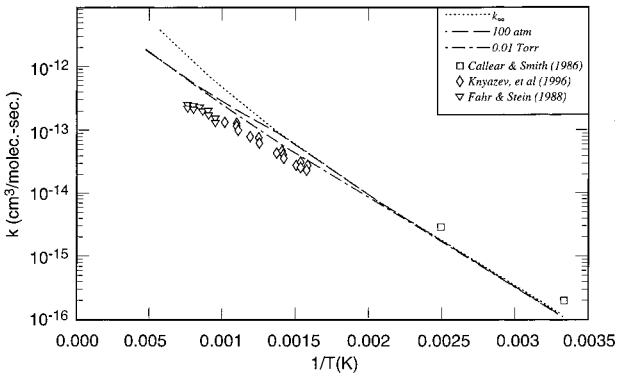

Figure 10. Arrhenius plot of $k_1(T,p)$ for the two-well master equation model using the DFT- B3LYP PES energies with E_{b3} reduced to −1 kcal/mol. See caption to Figure 8 for experimental results.

The pressure dependence of $k_1(T,p)$, as measured by the difference between $k_\infty(T)$ and $k_0(T)$, is determined by the relative sizes of E_{b1} and E_{b3}, the energies of transition states TS-1 and TS-3. The larger E_{b3} becomes for fixed E_{b1}, the greater is the pressure dependence of $k_1(T,p)$ in the low-temperature regime, $T < 700$ K. We are primarily interested in $E_{b1} > E_{b3}$. If we make E_{b1} significantly larger than E_{b3}, $k_\infty(T) \approx k_0(T)$ even though the product distribution may be a strong function of temperature and pressure. Figure 10 shows the results for a case where we have reduced E_{b3} from +2.7 kcal/mol to −1.0 kcal/mol. For this case, $k_0(T)$ and $k_\infty(T)$ are virtually indistinguishable up to $T \approx 500$ K, and they differ by only a factor of 4 at 2000 K. However, note that the "transition regime" between 700 K and 900 K remains for finite pressures (shown for $p = 100$ atm in the figure).

To obtain better agreement with experiment than is shown in Figures 8 and 10, we reduced E_{b1} from 5.72 to 5.22 kcal/

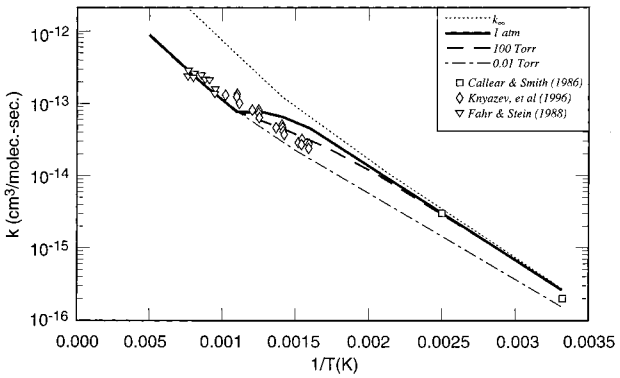

Figure 11. Arrhenius plot of $k_1(T,p)$ for the two-well master equation model using the DFT-B3LYP PES energies with E_{b1} reduced from 5.72 to 5.22 kcal/mol. See caption to Figure 8 for experimental results.

mol, retaining the other DFT PES parameters. The results are shown in Figure 11. The agreement between theory and experiment now is quite satisfactory. In this case, for 900 K < T < 2000 K, we can represent the rate coefficient $k_1(T)$ in the Arrhenius form,

$$k_1(T) = 2.19 \times 10^{-12} T^{0.163} \exp(-8312/RT)\ \mathrm{cm^3/(molecule{\cdot}s)}$$

independent of pressure.

Concluding Remarks

The results of the present investigation are remarkably similar to those of our previous study of the $C_2H_5 + O_2$ reaction.[26] In both cases there is a low-temperature regime where $x_R(t)$ decays exponentially in time, allowing the identification of a "good" rate coefficient, and the products behave normally, i.e., their time evolution is governed by the same time constant as $x_R(t)$. There follows a temperature regime, in the present case 700 K < T < 900 K, where nonexponential decays in $x_R(t)$ are the norm, at least at pressures sufficiently high that collisions of the intermediate complexes are significant. For T > 900 K (for the $C_2H_3 + C_2H_2$ reaction), $x_R(t)$ again decays exponentially, and the rate coefficient and products become independent of pressure, i.e.

$$C_2H_3 + C_2H_2 \rightarrow C_4H_4 + H$$

with $k_1(T) = k_0(T)$, the zero-pressure limit rate coefficient.

In the low-temperature regime the products are a complex function of both temperature and pressure. If the pressure is sufficiently high, going up in temperature can change the dominant product from n-C_4H_5 to c-C_4H_5 to $C_4H_4 + H$. There is generally a peak in the c-C_4H_5 concentration at $T \approx 700$ K. The i-C_4H_5 isomer is never an important product. However, for very high pressures it can peak at about 5% near $T = 800$ K.

Our results can be interpreted in terms of the eigenvalues and eigenvectors of the G matrix, the relaxation/reaction matrix of the master equation. At low temperatures, again at pressures sufficiently high that collisions are important, there are three eigenvalues of G that are significantly larger than the rest, and they are separated in magnitude from each other. At least approximately at low T, we can identify $-\lambda_1$ (where λ_1 is the largest eigenvalue) as the relaxation rate for the reaction n-C_4H_5 (or n-C_4H_5 and c-C_4H_5 combined) $\rightarrow C_4H_4 + H$, $-\lambda_2$ as that for n-$C_4H_5 \rightarrow$ c-C_4H_5, and $-\lambda_3$ as that for n-$C_4H_5 \rightleftarrows C_2H_3 + C_2H_2$. Starting at 300 K, as we increase the temperature, initially the rate coefficient is determined by λ_3. Very briefly, in the intermediate temperature regime, $k_1(T,p)$ is governed by λ_2. Then, above 900 K, λ_1 determines $k_1(T)$.

Our predictions are generally in good agreement with the experimental results available, limited as they are. Particularly good agreement can be obtained for the rate coefficients if we reduce the barrier height for TS-1 by 0.5 kcal/mol. In this case we can write $k_1(T)$ for 900 K < T < 2000 K as

$$k_1(T) = 2.19 \times 10^{-12} T^{0.163} \exp(-8312/RT)\mathrm{cm^3/(molec{\cdot}s)}$$

Acknowledgment. This work was supported by the United States Department of Energy, Office of Basic Energy Sciences, Division of Chemical Sciences.

References and Notes

(1) Miller, J. A. *Twenty-Sixth Symposium (International) on Combustion;* The Combustion Institute: Pittsburgh, PA, 1996; pp 461−480.
(2) Parker, C. L.; Cooksy, A. L. *J. Phys. Chem. A* **1999**, *103*, 2160−2169.
(3) Callear, A. B.; Smith, G. B. *Chem. Phys. Lett* **1984**, *105*, 119−122.
(4) Callear, A. B.; Smith, G. B. *J. Phys. Chem.* **1986**, *90*, 3229−3237.
(5) Fahr, A.; Stein, S. E. *Twenty-Second Symposium (International) on Combustion;* The Combustion Institute: Pittsburgh, PA, 1988; pp 1023−1029.
(6) Knyazev, V. D.; Stoliarov, S. I.; Slagle, I. R. *Twenty-Sixth Symposium (International) on Combustion;* The Combustion Institute: Pittsburgh, PA, 1996, pp 513−519.
(7) Wang, H.; Frenklach, M. *J. Phys. Chem.* **1994**, *98*, 11465−11489.
(8) Parker, C. L.; Cooksy, A. L. *J. Phys. Chem. A* **1998**, *102*, 6186−6190.
(9) Melius, C. F. Unpublished work.
(10) Curtiss, L. A.; Raghavachari, R.; Trucks, G. W.; Pople, J. A. *J. Chem. Phys.* **1991**, *94*, 7221.
(11) Curtiss, L. A.; Raghavachari, R.; Pople, J. A. *J. Chem. Phys.* **1993**, *98*, 1293.
(12) Bauschlicher, C. W.; Partridge, H. *J. Chem. Phys.* **1995**, *103*, 1788.
(13) Becke, A. D. *J. Chem. Phys.* **1993**, *98*, 5648.
(14) Dunning, T. H., Jr. *J. Chem. Phys.* **1989**, *90*, 1007. Kendall, R. A.; Dunning, T. H., Jr.; Harrison R. J. *J. Chem. Phys.* **1992**, *96*, 6796. Woon, D. E.; Dunning, T. H., Jr. *J. Chem.* Phys. **1993**, *98*, 1358.
(15) Frisch, M. J.; Trucks, G. W.; Schlegel, H. B.; Scuseria, G. E.; Robb, M. A.; Cheeseman, J. R.; Zakrzewski, V. G.; Montgomery, Jr., J. A.; Stratmann, R. E.; Burant, J. C.; Dapprich, S.; Millam, J. M.; Daniels, A. D.; Kudin, K. N.; Strain, M. C.; Farkas, O.; Ochterski, J.; Petersson, G. A.; Ayala, P. Y.; Cui, Q.; Morokuma, K.; Malick, D. K.; Rabuck, A. D.; Raghavachari, K.; Foresman, J. B.; Cioslowski, J.; Ortiz, J. V.; Stefanov, B. B.; Liu, G.; Liashenko, A.; Piskorz, P.; Komaromi, I.; Gomperts, R.; Martin, R. L.; Fox, D. J.; Keith, T.; Al-Laham, M. A.; Peng, C. Y.; Nanayakkara, A.; Gonzalez, C.; Challacome, M.; Gill, P. M. W.; Johnson, B.; Chen, W.; Wong, M. W.; Andres, J. L.; Gonzalez, C.; Head-Gordon, M.; Replogle, E. S.; Pople, J. A. *Gaussian 98, Revision A.6*; Gaussian, Inc.: Pittsburgh, PA, 1998.
(16) Frankcombe, T. J.; Smith, S. C.; Gates, K. E.; Robertson, S. H. *Phys. Chem. Chem. Phys.* **2000**, *2*, 793−803.
(17) Bedanov, V. M.; Tsang, W.; Zachariah, M. R. *J. Phys. Chem.* **1995**, *99*, 11452−11457.
(18) Tsang, W.; Bedanov, V.; Zachariah, M. R. *Ber. Bunsen-Ges. Phys. Chem.* **1997**, 491−499.
(19) Venkatesh, P. K.; Dean, A. M.; Cohen, M. H.; Carr, R. W. *J. Chem. Phys.* **1999**, *111*, 8313−8329.
(20) Gates, K. E.; Robertson, S. H.; Smith, S. C.; Pilling, M. J.; Beasley, M. S.; Maschhoff, K. J. *J. Phys. Chem. A* **1997**, *101*, 5765−5769.
(21) Barker, J. R. *Chem. Phys.* **1983**, *77*, 301.
(22) Shi, J.; Barker, J. R. *Int. J. Chem. Kinet.* **1990**, *22*, 187.
(23) Anderson, E.; Bai, Z.; Bishof, C.; Demmel, J.; Dongarra, J.; DuCroz, J.; Greenbaum, A.; Hammerling, S.; McKenney, A.; Ostronchov, S.; Sorensen, D. *LAPACK Users' Guide*; SIAM: Philadelphia, PA, 1992.
(24) Klippenstein, S. J.; Wagner, A. F.; Dunbar, R. C.; Wardlaw, D. M.; Robertson, S. H. Variflex Version 1.07m, Nov. 11, 1999.
(25) Miller, J. A.; Klippenstein, S. J., *J. Phys. Chem. A* **2000**, *104*, 2061−2069.
(26) Miller, J. A.; Klippenstein, S. J.; Robertson, S. H. A Theoretical Analysis of the Reaction Between Ethyl and Molecular Oxygen. *Twenty-Eighth Symposuim (International) on Combustion*; The Combustion Institute: Pittsburgh, PA, 2000; in press.
(27) Miller, J. A.; Parrish, C.; Brown, N. J. *J. Phys. Chem.* **1986**, *90*, 3339.
(28) Pitzer, K. S. *J. Chem. Phys.* **1946**, *14*, 239.

(29) Pitzer, K. S.; Gwinn, W. D. *J. Chem. Phys.* **1942**, *10*, 428.
(30) Widom, B. *Science* **1965**, *148*, 1555−1560.
(31) Widom, B. *J. Chem. Phys.* **1971**, *55*, 44−52.
(32) Widom, B. *J. Chem Phys.* **1974**, *61*, 672−680.
(33) Bartis, J. T.; Widom, B. *J. Chem. Phys.* **1974**, *60*, 3474−3482.
(34) Troe, J. *J. Chem. Soc., Faraday Trans*. **1994**, *90*, 2303−2317.
(35) Just, Th. *Twenty-Fifth Symposioum (International) on Combustion,* The Combustion Institute: Pittsburgh, PA, 1994; pp 687−704.